Materials and Design 103 (2016) 244–248

Contents lists available at ScienceDirect

Materials and Design

journal homepage: www.elsevier.com/locate/matdes

Mapping the strain and tilt of a suspended 3C-SiC membrane through micro X-ray diffraction

Gerard Colston [a,*], Stephen D. Rhead [a], Vishal A. Shah [b], Oliver J. Newell [a], Igor P. Dolbnya [c], David R. Leadley [a], Maksym Myronov [a]

[a] Department of Physics, University of Warwick, Coventry CV4 7AL, United Kingdom
[b] School of Engineering, University of Warwick, Coventry CV4 7AL, United Kingdom
[c] Diamond Light Source, Harwell Science and Innovation Campus, Didcot OX11 0DE, United Kingdom

ARTICLE INFO

Article history:
Received 15 January 2016
Received in revised form 19 April 2016
Accepted 23 April 2016
Available online 25 April 2016

Keywords:
3C-SiC
Membrane
Strain
Tilt
XRD

ABSTRACT

Micro X-ray diffraction (μ-XRD) has been used to map the strain profile of a suspended crystalline cubic Silicon Carbide (3C-SiC) square membrane. While the presence of crystal defects in the 3C-SiC epilayer induces significant errors on the position of the 3C-SiC Bragg peaks, relaxation from residual tensile strain can be observed and directly quantified from the XRD measurements. The advantage of μ-XRD over other strain mapping techniques is that the tilt of the crystalline layers can be measured simultaneously with the lattice parameters. Significant tilt variations have been observed at the corner of the 3C-SiC membrane, implying that the undercut from chemical etching induces distortions in the crystal structure. These distortions are likely to be the cause of the increase in strain commonly observed at the edges of suspended structures using the micro-Raman shift strain mapping technique.

1. Introduction

Silicon carbide (SiC) is a wide bandgap compound semiconductor with a high critical electric field and thermal conductivity [1]. This combination of properties makes SiC ideal for the fabrication of devices such as Schottky diodes and MOSFETs for use in high voltage power electronics [2]. The crystal structure of SiC can be formed from various stacking sequences of hexagonal Si-C bilayers, producing over 200 unique polymorphs. Of these, the hexagonal structured 4H-SiC is the prominent material found in commercially available SiC based power devices. However, the expensive bulk growth techniques required to produce 4H-SiC substrates and the subsequent homoepitaxial growth drives up the cost of SiC based power electronic devices.

An attractive solution to this issue of cost is through the use of the cubic structured 3C-SiC polytype, which can be heteroepitaxially grown by Chemical Vapour Deposition (CVD) on high quality crystalline silicon (Si) substrates, dramatically reducing production costs. Heteroepitaxial growth, however, is difficult due to two main issues. The huge lattice mismatch between the lattice constants of Si and 3C-SiC (19.7%) results in a misfit dislocation at every 5th 3C-SiC plane at the interface and as a result epilayers are plagued with stacking faults [3]. The differences in Thermal Expansion Coefficients (TEC) and strain mismatch between 3C-SiC and Si can lead to serious wafer bow which tends to increase with epilayer thickness and growth temperature [4]. Even with significant research and breakthroughs in the heteroepitaxial growth of 3C-SiC such as patterned substrates [5] or selective epitaxy [6], there exist no commercial 3C-SiC/Si based power devices due to the current leakage caused by the highly defected material and bowed epi wafers. In spite of this limitation, even highly defective 3C-SiC layers have unique applications in microelectromechanical systems (MEMS) operating in harsh environments [7]. The high melting point and chemical inertness as well as the ability to selectively etch away the Si substrate to form freestanding 3C-SiC structures and sensors gives 3C-SiC a unique advantage over other materials and SiC polytypes.

The effects of strain variation can have significant consequences on the physical properties of suspended 3C-SiC films and structures. One such example can be directly observed in the bending of suspended 3C-SiC cantilevers [8]. There have been some attempts to investigate the effects of strain on suspended 3C-SiC structures through the use of micro-Raman (μ-Raman) mapping [9,10]. In all cases, the 3C-SiC has been observed to undergo slight relaxation from residual tensile strain, caused by mismatch in TEC [11], upon suspension. Another interesting observation made on suspended 3C-SiC structures is an increase in strain located only at the interface between suspended and supported 3C-SiC in the undercut region. This has been shown to be caused by the activation of a shear stress at the undercut region [10,12].

The aim of this investigation was to measure the strain relaxation of a suspended 3C-SiC square membrane through the use of micro X-ray diffraction (μ-XRD), a method which has been previously applied to

* Corresponding author.
E-mail address: M.Myronov@warwick.ac.uk (M. Myronov).

http://dx.doi.org/10.1016/j.matdes.2016.04.078
0264-1275/

crystalline Ge membranes [13]. The direct measurement of the lattice parameters through the use of XRD would firstly corroborate the results observed through Raman peak shift, but in addition, can also give information regarding the localised tilt of the suspended structures.

2. Experimental

A 3C-SiC layer was epitaxially grown on an on-axis, 100 mm diameter, 525 μm thick Si (001) substrate by reduced-pressure chemical vapour deposition (RP-CVD) in an LPE ACIS M8 system using trichlorosilane ($SiHCl_3$), ethylene (C_2H_4) and hydrogen (H_2) as the silicon supply, carbon supply and gas carrier respectively. An initial carbonization step was performed at 1140 °C and was subsequently followed by growth of the 3C-SiC layer at 1350 °C using a C/Si ratio of 1.4 [14,15]. The carbonization process is required to form a buffer layer upon the Si surface to instigate the growth of 3C-SiC. Optimizing the buffer layer has been found to increase crystallinity and reduce surface roughness of 3C-SiC epilayers, as well as significantly reduce the density of voids at the 3C-SiC/Si interface [16]. Overall lattice parameters of the 3C-SiC epilayer were collected using a lab based Panalytical X'Pert Pro MRD diffractometer using Cu $K\alpha_1$ radiation with a wavelength of 1.5406 Å. The in- and out-of-plane lattice parameters were determined by (224) and (004) reciprocal space maps (RSMs) respectively. Cross-sectional transmission electron microscopy (X-TEM) measurements were performed using a JEOL JEM-2000FX TEM operating at 200 kV.

Prior to the membrane fabrication, the grown 3C-SiC layer was approximately 5 μm thick and under slight tensile strain (~0.1%), which arises during the epitaxial growth of 3C-SiC on Si; although the 3C-SiC layer is fully-relaxed at growth temperatures it becomes tensile strained during cooling due to the difference in the TEC of the 3C-SiC and Si [17,18]. While 5 μm is thick for typical MEMS structures, this thickness of 3C-SiC is required for achieving higher crystalline quality, reducing the defect density from $>10^6$ cm^{-1} down to ~10^4 cm^{-1} by the annihilation of stacking faults [19]. The 3C-SiC membrane is fabricated in several stages [20]. A 1.5 mm × 1.5 mm window, over which the 3C-SiC membrane was suspended, was first defined by optical lithography using the alkaline resistant photoresist ProTEK PSB on the underside of the unpolished Si substrate. Then, the sample was etched in a 25 wt.% tetramethylammonium hydroxide (TMAH) bath at 90 °C for 16 h allowing the TMAH to etch through the ~525 μm of Si. The TMAH selectively etches the {001} Si planes whereas the {111} planes are effectively etch resistant [21]. The ProTEK PSB and 3C-SiC are extremely etch-resistant to TMAH and as a result the 3C-SiC is suspended over a region of approximately 1.3 mm × 1.3 mm, due to the nature of the etching process, as seen in Fig. 1. The suspended membrane remains under tensile strain as it is fixed to the 3C-SiC-on-Si (001) frame. After suspension, the membrane was subject to a 5 min. Piranha etch (4:1 concentrated H_2SO_4 to 30%wt. H_2O_2) and a 30 s 2.5% HF dip to remove the photoresist and clean the 3C-SiC surface.

The μ-XRD experiments were performed on beamline B16 at the Diamond Light source [22] using X-rays with an energy of 14.6 keV (0.849 Å). A compound refractive lens was used to focus the X-ray beam to a spot size of ~2.5 μm full width half maximum (FWHM). The sample was mounted on top of an *XYZ* stage (with ~0.5 μm precision) in a five-circle diffractometer allowing the sample to be moved through the beam. Scattered X-rays were collected by a PILATUS 300 K area detector capable of mapping Bragg peaks in both 2θ (the scattering angle) and γ (the angle of the scattering plane in the horizontal direction). To locate the membrane the diffractometer was aligned on to a Si substrate Bragg peak and the disappearance of this peak was observed as the sample was moved to a position where the beam only impinged on the suspended 3C-SiC membrane. This experimental set-up allows one to perform lines scans along the [110] direction across the middle of the sample where RSMs were obtained by rocking ω (the angle of incidence) around the Bragg reflection at each spatial point as the sample was rastered through the beam, as seen in Fig. 1. This experimental set-up gives intensity with respect to three variables (2θ, γ and ω). Fitting to these variables gives the position of the Bragg peaks in the coordinates of the diffractometer, from which the out-of-plane ($q_\perp$) and in-plane ($q_{||}$) scattering vectors can be calculated using [23]

$$q_\perp = \frac{2}{\lambda} sin(\theta)\, cos((\omega - \gamma) - \theta - tilt), \tag{1}$$

$$q_{||} = \frac{2}{\lambda} sin(\theta)\, sin((\omega - \gamma) - \theta - tilt) \tag{2}$$

where the tilt of the epilayer relative to the substrate is only applied to the asymmetric (115) RSM, and calculated by

$$tilt = atan\left(\frac{q_{||}}{q_\perp}\right)_{(004)}. \tag{3}$$

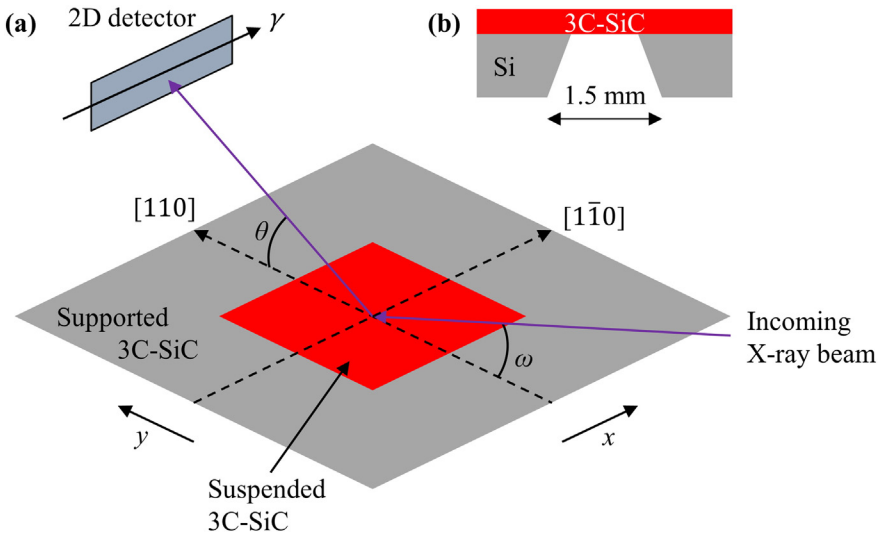

Fig. 1. (a) XRD scattering geometry for the acquisition of (004) RSMs. (b) Schematic cross-section of a 1.3 mm × 1.3 mm × 5 μm 3C-SiC membrane fabricated by selective wet etching.

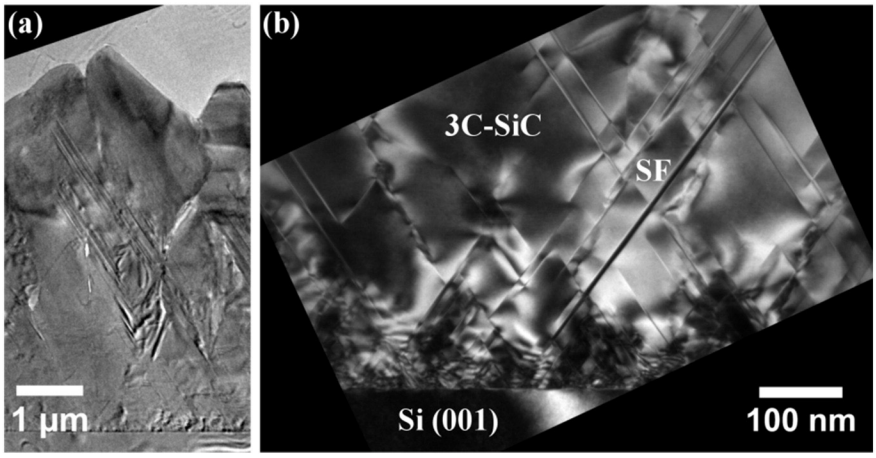

Fig. 2. (a) Cross-sectional TEM micrograph of the 3C-SiC layer on Si (001) substrate. (b) (220) dark field micrograph illustrating the large number of stacking faults (SF) originating at the interface between the 3C-SiC layer and Si (001) substrate.

The in- and out-of-plane lattice parameters ($a_{\parallel}$ and $a_{\perp}$ respectively) were determined from (115) RSMs, after being corrected for the tilt (measured from the (004) RSMs), using

$$a_{\parallel} = \frac{\sqrt{2}}{q_{\parallel}}\ a_{\perp} = \frac{5}{q_{\perp}}. \tag{4}$$

For these experiments the sample was mounted on a fine XY translation piezo stage, situated on top of the XYZ stage. The addition of the piezo stage allows fast 2D maps to be generated; a 95 μm × 95 μm region is scanned in 5 μm increments for a given ω. Upon completion ω is incremented and the process repeated. This process continues until ω is scanned across the Si and 3C-SiC (004) peaks. Such a map can be obtained in approximately half the time compared to the generation of the same map from a series of line scans. Due to the large lattice mismatch between Si and 3C-SiC there is a large separation of the Bragg peaks in reciprocal space. As a result of this, separate RSMs around the Si and 3C-SiC peaks were performed with the detector centred on the Si and 3C-SiC 2θ respectively. For both scan types the spatial resolution in real space is given by the beam spot-size.

3. Results and discussion

Typical X-TEM micrographs of the 3C-SiC layers as grown are displayed in Fig. 2. The 3C-SiC is approximately 5 μm thick and has poor surface morphology due to faceted growth and lack of post growth surface polishing. The stacking fault density in the 3C-SiC epilayers is over 10^5 cm^{-1}, as measured from X-TEM (Fig. 2b), typical of near 3C-SiC/Si substrate interface defect densities [19]. Lab-based symmetric (004) and asymmetric (224) RSMs from the as-grown 3C-SiC on Si (001) substrates are shown in Fig. 3a and b respectively. The in-plane ($a_{\parallel}$) and out-of-plane ($a_{\perp}$) lattice parameters for 3C-SiC are found to be $a_{\parallel} = 4.3639$ Å and $a_{\perp} = 4.3555$ Å respectively. The in- and out-of-plane strain ($\varepsilon_{\parallel}$ and $\varepsilon_{\perp}$ respectively) are calculated using

$$\varepsilon_{\parallel} = \frac{a_{\parallel} - a_{SiC}}{a_{SiC}} = \frac{-2C_{12}}{C_{11}}\ \frac{a_{\perp} - a_{SiC}}{a_{SiC}} = \frac{-2C_{12}}{C_{11}}\ \varepsilon_{\perp}, \tag{5}$$

where a_{SiC} is the relaxed lattice parameter of 3C-SiC ($a_{SiC} = 4.3596$ Å) and C_{11} and C_{12} are elastic constants of 3C-SiC [24]. The 3C-SiC is slightly tensile strained with $\varepsilon_{\parallel} = (0.099 \pm 0.003)$ %, $\varepsilon_{\perp} = (-0.094 \pm 0.002)$ %,

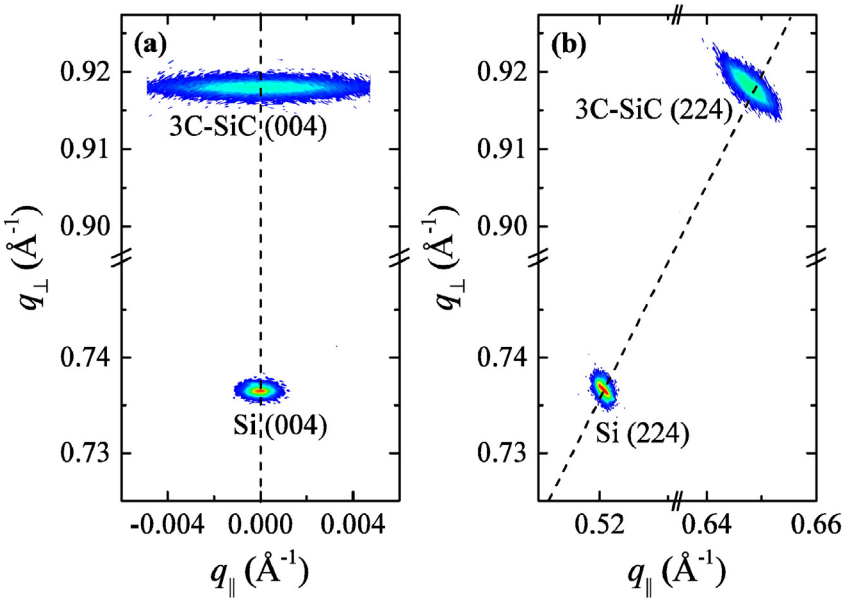

Fig. 3. Lab-based 3C-SiC (a) symmetric (004) and (b) asymmetric (224) RSMs. The scattering vectors are defined as $q_{\perp} = 4/a_{\perp}$ for both reflections and for the (224) only $q_{\parallel} = 2\sqrt{2}/a_{\parallel}$. The dashed lines indicate the expected positions of the Bragg peaks for (a) un-tilted and (b) fully relaxed layers. The shift of the 3C-SiC (224) Bragg peak indicates residual tensile strain in the epilayer.

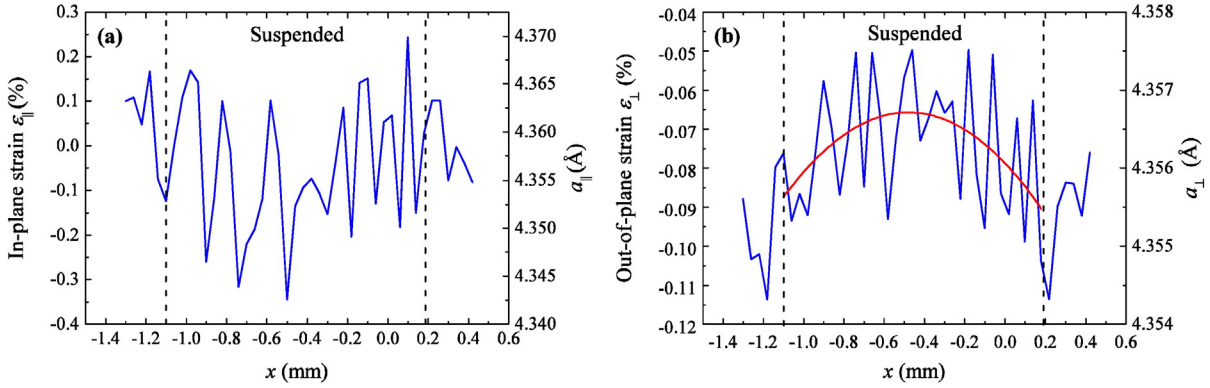

Fig. 4. In-plane (a) and out-of-plane (b) strain profiles across the centre of the 3C-SiC membrane calculated from tilt corrected (115) RSMs. The borders of the membrane are highlighted by the locations of the dashed lines.

allowing for the formation of suspended membranes. Although no significant wafer tilt is observed due to the large lab-based XRD spot size as the diffracted signal is averaged over several mm, a visual inspection confirmed the wafer's bow. The large FWHM of the 3C-SiC peaks confirms the presence of a large number of defects in the epilayer.

Symmetric (004) and asymmetric (115) RSMs were acquired at various points across the 1.3 mm × 1.3 mm 3C-SiC membrane by μ-XRD so as to map the Si and 3C-SiC Bragg peaks in a linescan profile through the centre of the membrane and onto the supporting bulk Si along the [110] direction. The in- and out-of-plane strain profiles are shown in Fig. 4. While both profiles are dominated by noise, the uncertainties of the in-plane profile are far more significant and are exaggerated by the calculation of lattice parameters from the (115) RSMs, see Eq. (4). The use of (224) RSMs would decrease this error as variations in $q_{||}$ would be larger and the Bragg diffraction intensity is larger due to the (224) reflection has a stronger structure factor, however, these were not feasible with the experimental set-up. The out-of-plane strain suffers from less noise and a profile can be observed with the strain varying from $\varepsilon_{\perp} = (-0.09 \pm 0.01)$ % on the supported edges to $\varepsilon_{\perp} = (-0.07 \pm 0.01)$ % in the central 25% of the suspended membrane. The errors were calculated by taking the standard deviation from the mean of the strain values in each specified region. Although no profile can be directly ascertained from Fig. 4a, it is safe to assume that the in-plane strain varies with the out-of-plane strain according to Eq. (5) for the central region of the membrane, which will exhibit biaxial strain. This implies that upon suspension the membrane itself undergoes partial relaxation from residual tensile strain. This result is in agreement with those found in literature using μ-Raman strain mapping techniques previously described [10,12].

The variation of epilayer tilt was mapped over the corner of the membrane by acquiring symmetric (004) RSMs using a piezo scan. In this case, the tilt is defined as the variation of the crystalline orientation of a layer relative to itself. For this, a reference point was taken on the bulk region of the 3C-SiC/Si and defined to have a tilt of zero. The tilt variation of the Si and 3C-SiC can be seen in Fig. 5. The tilt map of the 3C-SiC epilayer (Fig. 5b) is dominated by noise, a result of the high density of stacking faults in the crystal which dramatically broadens the 3C-SiC Bragg peak in $q_{||}$ (see Fig. 3a). The tilt map of the Si, however, shows a distinct variation at the border of the membrane. Assuming that the 3C-SiC epilayer remains bound to the Si over this region, this would imply that the 3C-SiC must also exhibit the same variation in tilt which would cause the shear strain found at the undercut of the Si substrate [10]. As Raman measurements neglect crystalline tilt, this effect can easily be misinterpreted as an increase in tensile strain simply by mapping Raman peak shift. A similar effect has been observed at the edges of Ge membranes and used to justify why the membrane undergoes a slight increase in tensile strain [13]. In the case of 3C-SiC, however, it would appear the removal of the underlying Si substrate dominates in removing the tensile strain brought about by wafer bow, which explains why the majority of the suspended 3C-SiC exhibits

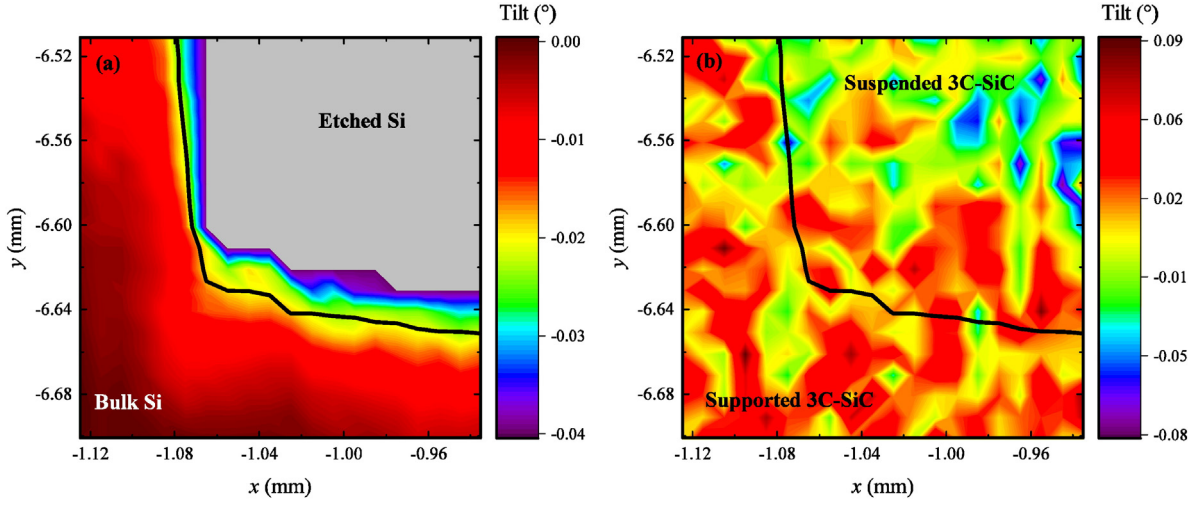

Fig. 5. The tilt of the underlying Si (a) and the 3C-SiC epilayer (b) at the corner of the membrane, calculated from (004) RSMs. The tilt is defined as the orientation of a crystalline layer relative to itself, for each layer (3C-SiC and Si) the reference point was taken at (−1.125, −6.701) with the tilt at this point defined as zero. The black line indicates the point at which the Si Bragg peak intensity has dropped by 50%, and hence the corner of the membrane.

strain relaxation while edge effects can induce a localised increase in shear strain caused by crystalline tilt.

4. Conclusion

In conclusion, micro X-ray diffraction (μ-XRD) techniques have been used to map the strain and tilt variation across a suspended 3C-SiC membrane, heteroepitaxially grown on Si (001). Strain relaxation is observed across the membrane which is in agreement with data from other investigations that have relied on Raman shift measurements. In the case of 3C-SiC, crystalline defects significantly increase the noise of the XRD data and as such, for these types of measurements, μ-Raman is a more suitable measurement technique. The key advantage of using μ-XRD over μ-Raman shift is that the shifting of Raman peaks cannot give any information on the tilt of the crystalline layers. As 3C-SiC grown on Si remains a highly defective material a direct measurement of the 3C-SiC tilt cannot be made, however, by analysing the tilt of the underlying Si substrate it is possible to indirectly assess the 3C-SiC tilt at the edges of the membrane up until the 3C-SiC is fully suspended. This relies on the assumption that the 3C-SiC remains bonded to the underlying Si and undergoes the same physical deformations as the substrate. These measurements have revealed a significant change in the crystalline tilt at the location of the undercut caused by the chemical etching process. This suggests that the increase in shear strain, found at the transition from supported to suspended 3C-SiC, observed in μ-Raman measurements is due to slight distortions of the 3C-SiC/Si at the point the epilayer becomes fully suspended. The removal of the underlying Si substrate for the rest of the membrane, however, dominates in reducing the tensile strain induced by the mismatch in TECs, resulting in the partial relaxation of the suspended 3C-SiC as a whole.

Acknowledgements

This research was supported by STFC-funded MT11773 and MT10303 projects. The Diamond Light Source is acknowledged for providing beamtime.

References

[1] S.E. Saddow, A. Agarwal, Advances in Silicon Carbide Processing and Applications, first ed. Artech House Inc., Norwood, MA 02062, 2004.
[2] M. Ostling, R. Ghandi, C.M. Zetterling, Ieee, 2011 Ieee 23rd International Symposium on Power Semiconductor Devices and Ics, 2011 10.
[3] A. Severino, C. Frewin, C. Bongiorno, R. Anzalone, S.E. Saddow, F. La Via, Diam. Relat. Mater. 18 (2009) 1440, http://dx.doi.org/10.1016/j.diamond.2009.09.012.
[4] M. Zielinski, S. Ndiaye, T. Chassagne, S. Juillaguet, R. Lewandowska, M. Portail, A. Leycuras, J. Camassel, Phys. Status Solidi (a) 204 (2007) 981, http://dx.doi.org/10.1002/pssa.200674130.
[5] H. Nagasawa, K. Yagi, T. Kawahara, N. Hatta, Chem. Vap. Depos. 12 (2006) 502, http://dx.doi.org/10.1002/cvde.200506466.
[6] A. Gupta, C. Jacob, Prog. Cryst. Growth Charact. Mater. 51 (2005) 43, http://dx.doi.org/10.1016/j.pcrysgrow.2005.10.003.
[7] C.A. Zorman, R.J. Parro, Phys. Status Solidi B Basic Solid State Phys. 245 (2008) 1404, http://dx.doi.org/10.1002/pssb.200844135.
[8] M. Bosi, B.E. Watts, G. Attolini, C. Ferrari, C. Frigeri, G. Salviati, A. Poggi, F. Mancarella, A. Roncaglia, O. Martínez, V. Hortelano, Cryst. Growth Des. 9 (2009) 4852, http://dx.doi.org/10.1021/cg900677c.
[9] R. Anzalone, G. D'Arrigo, M. Camarda, N. Piluso, F.L. Via, Mater. Sci. Forum 778-780 (2014) 457.
[10] N. Piluso, R. Anzalone, M. Camarda, A. Severino, A. Magna, G. D'Arrigo, F. La Via, J. Raman Spectrosc. 44 (2013) 299, http://dx.doi.org/10.1002/jrs.4171.
[11] S. Rohmfeld, M. Hundhausen, L. Ley, C.A. Zorman, M. Mehregany, J. Appl. Phys. 91 (2002) 1113, http://dx.doi.org/10.1063/1.1427408.
[12] N. Piluso, R. Anzalone, M. Camarda, A. Severino, G. D'Arrigo, F. La Via, Thin Solid Films 522 (2012) 20, http://dx.doi.org/10.1016/j.tsf.2011.12.078.
[13] S.D. Rhead, J.E. Halpin, V.A. Shah, M. Myronov, D.H. Patchett, P.S. Allred, V. Kachkanov, I.P. Dolbnya, J.S. Reparaz, N.R. Wilson, C.M.S. Torres, D.R. Leadley, Appl. Phys. Lett. 104 (2014) 5, http://dx.doi.org/10.1063/1.4874836.
[14] R. Anzalone, A. Severino, G. D'Arrigo, C. Bongiorno, G. Abbondanza, G. Foti, S. Saddow, F. La Via, J. Appl. Phys. 105 (2009) 084910, http://dx.doi.org/10.1063/1.3095462.
[15] R. Anzalone, A. Alberti, F. La Via, Mater. Lett. 118 (2014) 130, http://dx.doi.org/10.1016/j.matlet.2013.12.067.
[16] M. Bosi, G. Attolini, M. Negri, C. Frigeri, E. Buffagni, C. Ferrari, T. Rimoldi, L. Cristofolini, L. Aversa, R. Tatti, R. Verucchi, J. Cryst. Growth 383 (2013) 84, http://dx.doi.org/10.1016/j.jcrysgro.2013.08.005.
[17] B.E. Watts, G. Attolini, M. Bosi, C. Frigeri, Mater. Lett. 62 (2008) 2129, http://dx.doi.org/10.1016/j.matlet.2007.11.066.
[18] G. Ferro, Crit. Rev. Solid State Mater. Sci. 40 (2014) 56, http://dx.doi.org/10.1080/10408436.2014.940440.
[19] F. La Via, Silicon Carbide Epitaxy, Research Signpost, Kerala, 2012.
[20] V.A. Shah, S.D. Rhead, J.E. Halpin, O. Trushkevych, E. Chávez-Ángel, A. Shchepetov, V. Kachkanov, N.R. Wilson, M. Myronov, J.S. Reparaz, R.S. Edwards, M.R. Wagner, F. Alzina, I.P. Dolbnya, D.H. Patchett, P.S. Allred, M.J. Prest, P.M. Gammon, M. Prunnila, T.E. Whall, E.H.C. Parker, C.M. Sotomayor Torres, D.R. Leadley, J. Appl. Phys. 115 (2014)http://dx.doi.org/10.1063/1.4870807.
[21] O. Tabata, R. Asahi, H. Funabashi, K. Shimaoka, S. Sugiyama, Sensors Actuators A Phys. 34 (1992) 51, http://dx.doi.org/10.1016/0924-4247(92)80139-T.
[22] K.J.S. Sawhney, I.P. Dolbnya, M.K. Tiwari, L. Alianelli, S.M. Scott, G.M. Preece, U.K. Pedersen, R.D. Walton, AIP Conf. Proc. 1234 (2010) 387, http://dx.doi.org/10.1063/1.3463220.
[23] G. Bauer, J.H. Li, E. Koppensteiner, J. Cryst. Growth 157 (1995) 61, http://dx.doi.org/10.1016/0022-0248(95)00372-x.
[24] W.R.L. Lambrecht, B. Segall, M. Methfessel, M. van Schilfgaarde, Phys. Rev. B 44 (1991) 3685.